AIAA JOURNAL
Vol. 45, No. 8, August 2007

Stochastic Buckling Analysis of Laminated Plates Under Shear and Compression

A. K. Onkar,* C. S. Upadhyay,† and D. Yadav‡
Indian Institute of Technology, Kanpur 208 016, India

DOI: 10.2514/1.25800

A stochastic finite-element-based prediction of the buckling of composite laminated plates, with and without cutouts, under axial compression and shear is presented. The solution for the buckling response is achieved by first evaluating the prebuckled-stress distribution from linear elastostatic analysis. Using this, the critical buckling load and its mode are evaluated by solving an eigenvalue problem. A layerwise plate model is used for both prebuckling and buckling analysis. The effect of prebuckling stresses on the critical buckling load is discussed. The influence of both circular and elliptical cutouts on the buckling strength of composite laminates is presented. The stochastic buckling analysis is done based on the mean-centered first-order perturbation technique. The mean and variance of the buckling strength of composite plates are validated with results available in the literature. Subsequently, the effect of uncertainty in the material properties, obtained from micromechanics-based approach, on the buckling strength of the laminated plates is studied. Results are presented for two-layered plates with different layups and boundary conditions.

Introduction

LAMINATED composites are gaining acceptance in the construction of components of automobile, aircraft, and launch vehicles. Their use has resulted in a significant increase in payload, weight reduction, and durability. Among many other components, flat plates are commonly used as parts of the stabilizers, wings, and fuselage. Sometimes, cutouts are made in these plates to serve as access ports to the mechanical and electrical devices. Because these components are subjected to in-plane forces combined with transverse pressure, the buckling response of such panels is a basic concern in the design process. These composite laminates generally display dispersion in the mechanical properties due to the complexities involved in the manufacturing process. In the presence of inherent scatter in the material properties, a statistical theory combined with traditional mechanics are widely used by researchers to quantify the response uncertainty.

An overview of past research related to the buckling of laminated plates with and without cutouts was carried out for both deterministic and stochastic problems. Most of the existing mean analytical buckling solutions [1–7], which use either the classical plate theory (CPT), the first-order shear deformation theory (FSDT), or the higher-order shear deformation theory (HSDT), are based on uniform prebuckled-state-of-stress assumptions. The reason for assuming the uniform prebuckled states of stress may be due to the complexity involved in analytically solving a problem of plane-stress elasticity for an accurate internal prestress distribution. However, this does not represent the true situation and leads to inaccuracy in the buckling analysis. Hence, many authors have used the finite element method to predict the accurate in-plane stress distribution, which is later used to solve the buckling problem [8–14]. The mean stability analysis of plates with cutouts has been studied by many investigators. Numerical investigation of the buckling behavior of both isotropic and composite plates with centrally located cutouts has been performed with various approaches and plate models using the finite element method [15–20]. The effect of the various shapes of a cutout (square, circular, elliptical, etc.), its location (eccentricity), and the size of a cutout on the mean buckling load has also been reported in [21–25].

To quantify the structural response uncertainty, a Taylor-series-expansion-based perturbation approach in conjunction with the finite element method has been widely used by researchers. The statistics of the buckling load of composite plates without a hole have been studied in [26–29]. The material properties, fiber angles, laminate thickness, and different in-plane random loads are treated as basic random variables (BRVs). Both the stochastic finite element method (SFEM) and Monte Carlo simulation (MCS) were used to quantify the structural response uncertainty. An overview of different stochastic methods has been presented for solving classical problems of solid mechanics in [30], with an elementary illustration of the perturbation-based stochastic finite element method. The effect of uncertainty in the initial geometric imperfections (such as radius and thickness) becomes important in the stochastic buckling analysis of shells. The stochastic finite element analysis of shell structures without cutouts has been performed for both uncertain material and geometric properties in conjunction with MCS to obtain the response variability [31,32].

In this paper, a stochastic finite element formulation-based on the mean centered first-order perturbation technique is presented for the buckling analysis of laminated composite plates under shear and compressive loading. The mean buckling analysis is done by first solving the linear elastic problem to get accurate prebuckling stresses and then these stresses are used in solving the eigenvalue problem for the lowest eigenvalue. A layerwise plate model is used to get the accurate state of prebuckled stresses in the plate. The effect of initial prebuckled stresses on the buckling strength of composite plates for different layups and boundary conditions was also investigated. The statistics of the buckling strength is determined by considering uncertainties in the material properties of composite laminates. The validation of the stochastic finite element approach is performed by comparing the results with analytical solutions available in the literature. The effect of both circular and elliptical cutouts on the mean and variance of the critical buckling load of laminated plates is discussed. The effects of aspect ratios and layup sequences, along with a change in the standard deviation (SD) of material properties, were investigated for different boundary conditions.

Stochastic Finite Element Buckling Formulation

Buckling analysis can be performed with a linear model by assuming that the prebuckling deformations are small. A linear elastostatic problem for a reference load is solved first, and then from

Received 12 June 2006; revision received 21 March 2007; accepted for publication 13 April 2007.

*Graduate Student, Department of Aerospace Engineering.
†Associate Professor, Department of Aerospace Engineering.
‡Professor, Department of Aerospace Engineering.

this equilibrium position, we perturb the system such that it becomes unstable. Here, we look for all buckling-load parameters λ for which the system goes to a new equilibrium position and from among all λ, the critical or minimum load parameter λ_{cr} is chosen. In this formulation, Green's strains are used, which take into account the effect of both in-plane and out-of-plane displacements. The components of strain in terms of displacement fields u_i are defined as

$$\{\varepsilon\} = \{\varepsilon^L\} + \{\varepsilon^{\mathrm{NL}}\}, \qquad \varepsilon_{ij}^L = \frac{1}{2}\left\{\frac{\partial u_i}{\partial x_j} + \frac{\partial u_j}{\partial x_i}\right\}$$
$$\varepsilon_{ij}^{\mathrm{NL}} = \frac{1}{2}\left\{\frac{\partial u_k}{\partial x_i}\frac{\partial u_k}{\partial x_j}\right\} \qquad (i,j,k = 1,\ldots,3) \tag{1}$$

where $\{\varepsilon^L\}$ denotes the linear strain and $\{\varepsilon^{\mathrm{NL}}\}$ is the geometric nonlinear strain.

Let the plate with a stochastic elasticity tensor field C_{ijkl} be subjected to some uniform reference in-plane load q_i^{ref}. The coordinate definitions, material direction of a typical lamina, and loading conditions are shown in Fig. 1. The total potential energy corresponding to the linear state of the system for uncertain stiffness is written as [28]

$$\Pi(u_i^{\mathrm{ref}}) = \frac{1}{2}\int_\Omega C_{ijkl}\varepsilon_{ij}^{\mathrm{ref}}\varepsilon_{kl}^{\mathrm{ref}}\,\mathrm{d}\Omega - \int_{\Gamma_1} q_i^{\mathrm{ref}}u_i^{\mathrm{ref}}\,\mathrm{d}\Gamma_1$$
$$(i,j,k,l = 1,\ldots,3) \tag{2}$$

where Ω denotes the undeformed configuration of the plate and its boundary is denoted by $\Gamma = \Gamma_0 \cup \Gamma_1$, Γ_0 denotes the Dirichlet part and Γ_1 denotes the Neumann part of the lateral boundary of the plate, $\varepsilon_{ij}^{\mathrm{ref}}$ denotes the linear strain defined by Eq. (1), and q_i^{ref} is the boundary traction. In the present analysis, the uniform reference loads $q_1^{\mathrm{ref}} = q^{\mathrm{ref}}$ and $q_2^{\mathrm{ref}} = q_3^{\mathrm{ref}} = 0$ are taken.

The exact solution minimizes Π on the set of all kinematically admissible functions denoted by V (i.e., $u \in V$ such that $V = \{u \in H^1(\Omega)\colon M(u) = 0 \text{ on } \Gamma_0\}$), which yields

$$\delta\Pi(u_i^{\mathrm{ref}}) = \int_\Omega C_{ijkl}\varepsilon_{ij}^{\mathrm{ref}}\delta\varepsilon_{kl}^{\mathrm{ref}}\,\mathrm{d}\Omega - \int_{\Gamma_1} q_i^{\mathrm{ref}}\delta u_i^{\mathrm{ref}}\,\mathrm{d}\Gamma_1 = 0$$
$$(i,j,k,l = 1,\ldots,3) \tag{3}$$

Using the Taylor-series-expansion-based first-order perturbation approach, the preceding equation can be separated into the zeroth- and first-order equations as follows [28]:

Zeroth order:

$$\int_\Omega C_{ijkl}^0\varepsilon_{ij}^{0(\mathrm{ref})}\delta\varepsilon_{kl}^{0(\mathrm{ref})}\,\mathrm{d}\Omega = \int_{\Gamma_1} q_i^{0(\mathrm{ref})}\delta u_i^{0(\mathrm{ref})}\,\mathrm{d}\Gamma_1$$
$$(i,j,k,l = 1,\ldots,3) \tag{4a}$$

First order:

$$\int_\Omega C_{ijkl}^0\varepsilon_{ij}^{,r(\mathrm{ref})}\delta\varepsilon_{kl}^{0(\mathrm{ref})}\,\mathrm{d}\Omega = -\int_\Omega C_{ijkl}^{,r}\varepsilon_{ij}^{0(\mathrm{ref})}\delta\varepsilon_{kl}^{0(\mathrm{ref})}\,\mathrm{d}\Omega$$
$$(r = 1,\ldots,R) \tag{4b}$$

where R is the number of BRVs chosen for the analysis; $(\cdot)^0$ represents the function at the mean value of the input random variables; $(\cdot)^{,r}$ stands for the first-order partial derivative with respect to the input random variables b_r; zeroth-order equations give the mean response $u_i^{0(\mathrm{ref})}$; and first-order equations give the first-order response derivative $u_i^{,r(\mathrm{ref})}$. Having solved for $u_i^{(\mathrm{ref})}$ using $u_i^{0(\mathrm{ref})}$ and $u_i^{,r(\mathrm{ref})}$, one can also obtain the state of stresses $\sigma_{ij}^{\mathrm{ref}}$ by employing the linear stress–strain relationship.

Now from this equilibrium position, we perturb the system by an amount u_i^p (with strain ε_{ij}^p) such that the system becomes neutrally stable. The total potential energy of the perturbed system is written as

$$\Pi(u_i^p) = \int_\Omega \sigma_{ij}^{\mathrm{cr}}\varepsilon_{ij}^p\,\mathrm{d}\Omega + \frac{1}{2}\int_\Omega \sigma_{ij}^p\varepsilon_{ij}^p\,\mathrm{d}\Omega - \int_{\Gamma_1} q_i^{\mathrm{cr}}u_i^p\,\mathrm{d}\Gamma_1$$
$$(i,j = 1,\ldots,3) \tag{5}$$

where $\sigma_{ij}^{\mathrm{cr}}$ is the current linear state of stress due to the critical load $q^{\mathrm{cr}} = \lambda_{\mathrm{cr}}q^{\mathrm{ref}}$ and is given by $\sigma_{ij}^{\mathrm{cr}} = \lambda_{\mathrm{cr}}\sigma_{ij}^{\mathrm{ref}}$.

Upon substituting the perturbational strain ε_{ij}^p from Eq. (1) and linearizing the preceding equation, we have

$$\Pi(u_i^p) = \frac{1}{2}\int_\Omega C_{ijkl}\varepsilon_{ij}^{(L)p}\varepsilon_{kl}^{(L)p}\,\mathrm{d}\Omega + \lambda_{\mathrm{cr}}\int_\Omega \sigma_{ij}^{(\mathrm{ref})}\varepsilon_{ij}^{(\mathrm{NL})p}\,\mathrm{d}\Omega$$
$$(i,j,k,l = 1,\ldots,3) \tag{6}$$

where $\varepsilon_{ij}^{(L)p}$ is the linear part and $\varepsilon_{ij}^{(\mathrm{NL})p}$ is the nonlinear part of the perturbational strain ε_{ij}^p. Now λ_{cr} is found and $u \in V$, $u \neq 0$ such that Π is minimum, which yields

$$\delta\Pi(u_i^p) \equiv \int_\Omega C_{ijkl}\varepsilon_{ij}^{(L)p}\delta\varepsilon_{kl}^{(L)p}\,\mathrm{d}\Omega + \lambda_{\mathrm{cr}}\int_\Omega \sigma_{ij}^{(\mathrm{ref})}\delta\varepsilon_{ij}^{(\mathrm{NL})p}\,\mathrm{d}\Omega = 0$$
$$(i,j,k,l = 1,\ldots,3) \tag{7}$$

Similarly, the zeroth- and first-order variational equations are obtained from the preceding equation, using Taylor-series-expansion-based stochastic variational principles as follows [28]:

Zeroth order:

$$\int_\Omega C_{ijkl}^0\varepsilon_{ij}^{0(L)}\delta\varepsilon_{kl}^{0(L)}\,\mathrm{d}\Omega + \lambda_{\mathrm{cr}}^0\int_\Omega \sigma_{ij}^{0(\mathrm{ref})}\delta\varepsilon_{ij}^{0(\mathrm{NL})}\,\mathrm{d}\Omega = 0$$
$$(i,j,k,l = 1,\ldots,3) \tag{8a}$$

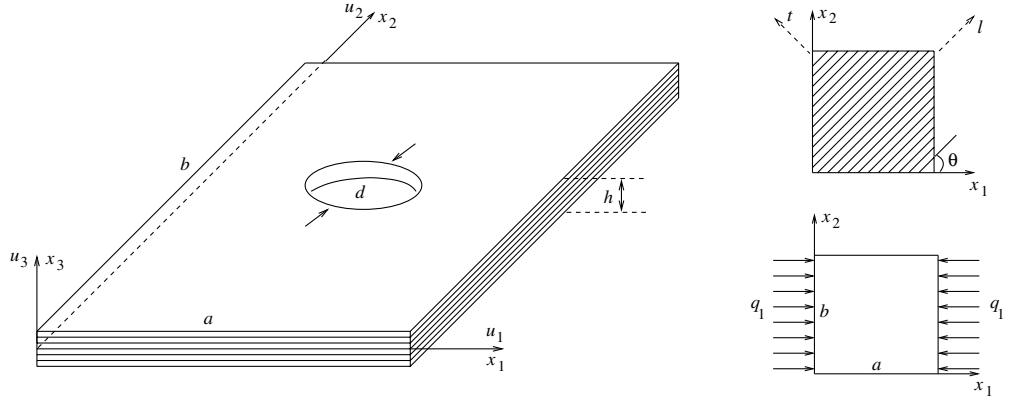

Fig. 1 Geometry of a laminated plate with centrally located cutout (left), lamina with material coordinates *l* and *t* (top right), and loading conditions (bottom right).

First order:

$$\int_\Omega \left(C^{,r}_{ijkl}\varepsilon^{0(L)}_{ij} + C^{0}_{ijkl}\varepsilon^{,r(L)}_{ij}\right)\delta\varepsilon^{0(L)}_{kl}\,\mathrm{d}\Omega + \lambda^{0}_{\mathrm{cr}}\int_\Omega \sigma^{,r(\mathrm{ref})}_{ij}\delta\varepsilon^{0(\mathrm{NL})}_{ij}\,\mathrm{d}\Omega + \lambda^{,r}_{\mathrm{cr}}\int_\Omega \sigma^{0(\mathrm{ref})}_{ij}\delta\varepsilon^{0(\mathrm{NL})}_{ij}\,\mathrm{d}\Omega = 0 \quad (i,j,k,l=1,\ldots,3;r=1,\ldots,R) \tag{8b}$$

Here, the superscript p was dropped from the preceding equations for the sake of clarity.

Discretization

In the present layerwise finite element discretization of the laminated plates, 3-D prismatic elements are used for which the projection on plane x_1–x_2 is a triangle. The layerwise displacement fields at any point in the laminate can be represented as [33]

$$\begin{aligned} u_1(x_1,x_2,x_3) &= U_{ij}N_i(x_1,x_2)\varphi_j(x_3)\\ u_2(x_1,x_2,x_3) &= V_{ij}N_i(x_1,x_2)\varphi_j(x_3)\\ u_3(x_1,x_2,x_3) &= W_{ij}N_i(x_1,x_2)\varphi_j(x_3)\\ (i=1,\ldots,n_{x_1x_2};&\ j=1,2,\ldots,n_{x_3}) \end{aligned} \tag{9}$$

where $n_{x_3} = nslay \times p_{x_3} + 1$, and $nslay$ is the total number of solution layers in the laminate. A solution layer herein means an entity generated by discretizing the plate along the thickness direction and may not necessarily represent a physical (or material) layer. It may represent a subdivision of a physical layer into sublaminas or may consist of number of physical layers lumped into a single solution layer, termed as an equivalent-solution layer (see Figs. 2a and 2b). $N_i(x_1,x_2)$ and $\varphi_j(x_3)$ are the 2-D and 1-D Legendre shape functions; U_{ij}, V_{ij}, and W_{ij} are the coefficients of the displacement components; and $n_{x_1x_2}$ is the total number of degrees of freedom in the x_1–x_2 plane and depends on the order of the in-plane approximation $p_{x_1x_2}$. If $\varphi_j(x_3)$ is defined over the thickness of the laminate (i.e., $n_{x_3} = p_{x_3} + 1$), then the model of Eq. (9) reduces to an "equivalent-layer" model (i.e., the transverse functions are taken to be smooth polynomials in terms of x_3 over all the laminas, as shown in Fig. 2a). Note that here we have taken the order of transverse approximation p_{x_3} to be same for u_1, u_2, and u_3. This is because the buckling problem has both the membrane (the prebuckled stress due to in-plane loading) and the bending effects (the buckled mode). To resolve these effects, p_{x_3} should be the same for all of the displacement components [34].

Upon substituting the preceding finite element approximation into the zeroth- and first-order variational equations (8a) and (8b) and by employing nonlinear Green's strain-displacement relationships, the discretized finite element system equations are written as follows:

Zeroth order:

$$\left(K^0_{ij} + \lambda^0_k K^{(G)0}_{ij}\right)\Delta^{k(0)}_j = 0 \qquad (i,j,k=1,2,\ldots,n) \tag{10a}$$

First order:

$$\left(K^0_{ij} + \lambda^0_k K^{(G)0}_{ij}\right)\Delta^{k,r}_j + \left(K^{,r}_{ij} + \lambda^0_k K^{(G),r}_{ij} + \lambda^{,r}_k K^{(G)0}_{ij}\right)\Delta^{k(0)}_j = 0 \quad (i,j,k=1,2,\ldots,n;\ r=1,2,\ldots,R) \tag{10b}$$

where K^0_{ij} and $K^{(G)0}_{ij}$ are the mean of the elastic and the geometric stiffness matrices, respectively; $K^{,r}_{ij}$ and $K^{(G),r}_{ij}$ denote the first-order partial derivatives of the corresponding stiffness matrices; and $\Delta^{k(0)}_j$ and $\Delta^{k,r}_j$ represent the mean and the first-order partial derivative of the kth eigenvector, composed of $\{U^0_{\mathrm{lm}}, V^0_{\mathrm{lm}}, W^0_{\mathrm{lm}}\}$ and $\{U^{,r}_{\mathrm{lm}}, V^{,r}_{\mathrm{lm}}, W^{,r}_{\mathrm{lm}}\}$ components, respectively. It may be noted that λ^0_{cr} is the minimum among all λ^0_i.

The zeroth-order equation (10a) represents a generalized eigenvalue problem that is solved for the mean critical buckling load. In some cases, $K^{(G)0}_{ij}$ is found to be positive semidefinite when shift-invert transformation is used to solve the eigenvalue problem. Then the rightmost eigenvalue gives the minimum value of the buckling load. The first-order equation is used to calculate the first-order partial derivatives of the eigenvalue with respect to the basic random variables. Having solved Eq. (10a) for the critical mean eigenvalue λ^0_{cr} and the corresponding mean eigenvector Δ^0_i, we premultiply both sides of Eq. (10b) by the mean eigenvector Δ^0_i, which gives

$$\Delta^0_i\left(K^0_{ij} + \lambda^0_{\mathrm{cr}}K^{(G)0}_{ij}\right)\Delta^{,r}_i = -\lambda^{,r}_{\mathrm{cr}}\left(\Delta^0_i K^{(G)0}_{ij}\Delta^0_j\right) - \Delta^0_i\left(K^{,r}_{ij} + \lambda^0_{\mathrm{cr}}K^{(G),r}_{ij}\right)\Delta^0_j \tag{11}$$

Because both K^0_{ij} and $K^{(G)0}_{ij}$ are symmetric, the left-hand side equals zero by the definition of the zeroth-order equation. Employing $K^{(G)0}_{ij}$ orthonormality conditions, the first term on the right-hand side reduces to $\lambda^{,r}_{\mathrm{cr}}$.

The expression for the first-order eigenvalue then takes the following form:

$$\lambda^{,r}_{\mathrm{cr}} = -\Delta^0_i\left(K^{,r}_{ij} + \lambda^0_{\mathrm{cr}}K^{(G),r}_{ij}\right)\Delta^0_j \quad (i,j=1,2,\ldots,n;\ r=1,2,\ldots,R) \tag{12}$$

The minimum eigenvalue or load parameter can be obtained as follows:

$$\lambda_{\mathrm{cr}}(b_r) = \lambda^0_{\mathrm{cr}}\left(b^0_r\right) + \lambda^{,r}_{\mathrm{cr}}\left(b^0_r\right)\left(b_r - b^0_r\right) \qquad (r=1,2,\ldots,R) \tag{13}$$

The second-order statistics of eigenvalue can be evaluated by first squaring and then taking expectation of the preceding equation. The statistics of the buckling load are obtained by multiplying the statistics of the critical load parameter with the reference load.

Numerical Results

The results for buckling strength statistics of laminated plates with and without cutouts are presented in this section. A layerwise-based stochastic finite element method is used. First, some of the prebuckled behavior of the laminated plates under uniform normal

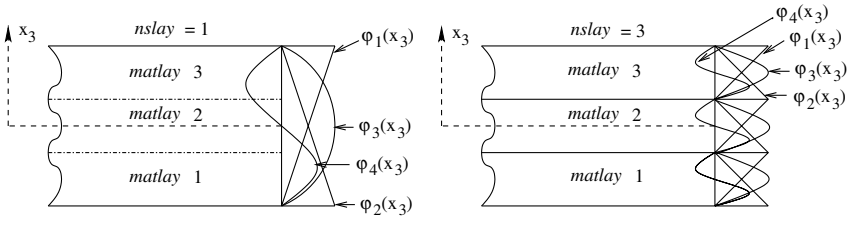

a) b)

Fig. 2 Representation of the transverse function over the thickness of the plate: a) equivalent layer and b) layer by layer.

Table 1 Different boundary conditions

Boundary condition	At $x_1 = 0$ and $x_1 = a$	At $x_2 = 0$ and $x_2 = b$
SSSS	$u_2 = u_3 = 0$	$u_1 = u_3 = 0$
SCSC	$u_2 = u_3 = 0$	$u_1 = u_2 = u_3 = 0$
SFSF	$u_2 = u_3 = 0$	$q_1 = q_2 = q_3 = 0$
HDSS	$u_1 = u_3 = 0$	$u_2 = u_3 = 0$

and shear loading is discussed. Based on these prebuckled studies, the mean buckling behavior of the plates is described. Further, the effect of randomness in material properties on the plate buckling load is investigated. The solutions developed for the mean and variance of the buckling loads of plates are verified with available results in the literature. The layer-by-layer model adopted for the analysis uses $p_{x_1x_2} = 3$ and $p_{x_3} = 1$, along with an appropriate mesh. Different types of boundary conditions, such as SSSS, SCSC, and SFSF used for plates under compressive loading and HDSS (hard simple support) used for plates under shear loading, are defined in Table 1.

Prebuckled Stress

In this section, the evaluation approach for the prebuckled stresses of composite laminates with and without cutouts is demonstrated with two-layered antisymmetric laminated plates $[-\theta/\theta]$. The effect of boundary conditions and aspect ratios of plates on the prebuckled-stress intensity $\bar{\sigma}_{ij} = \sigma_{ij}/q^{\text{ref}}$ is also obtained. Although all six components of stresses exist in the plate under traction loading, band plots of the prebuckled-stress distribution are drawn only for in-plane stress $\bar{\sigma}_{11}$ at the bottom face of the plates.

Results are presented for graphite/epoxy-laminated plates with $b/h = 50$ and having the following mean material properties: $E_{11} = 132.5$ GPa, $E_{22} = E_{33} = 10.8$ GPa, $G_{23} = 3.4$ GPa, $G_{12} = G_{13} = 5.7$ GPa, $\nu_{12} = \nu_{13} = 0.24$, $\nu_{23} = 0.49$, and $t_{\text{ply}} = 0.127$ mm.

The distribution of intensity of $\bar{\sigma}_{11}$ for plates with $\theta = 30$ and 60 deg with aspect ratio $a/b = 1$ and 2 are depicted in Figs. 3a, 3b, 4a, and 4b, respectively. Here, only two values of θ are taken, to economize space. The plates are supported with SSSS boundaries and subjected to uniform uniaxial compressive loading. It is observed that

1) There is a reduction of $\bar{\sigma}_{11}$ toward the center of the plate. This reduction is more pronounced for plates with $\theta > 30$ deg.

2) For 60-deg ply orientation, the stress reduction toward the center of the plate is very high and the stress value in most of the central region is equal to 0.16–0.32 times the applied load (see Fig. 3b).

3) This reduction in stress becomes more pronounced at a higher plate aspect ratio. For example, for plates with 60-deg ply orientation and $a/b = 2$, the stress value in most of the central region is equal to 0.0–0.16 times the applied load (see Fig. 4b).

Diffusion in prebuckled stresses is mainly due to the boundary constraints. Such diffusion in the intensity of stress is also found for plates having the SCSC boundary condition (figure not shown). However, in the case of plates with SFSF boundary constraints, diffusion in the prebuckled stress is not pronounced and the stress value is found to be equal to the applied load in most of the central region of the plate, except at the free edge, for which slight diffusion exists. This is because the SFSF boundary condition is a softer constraint than the SSSS and SCSC boundary constraints.

The effect of boundary constraints and layups on prebuckled stress for laminated plates in the presence of a cutout is also studied. Figures 5a and 5b show the distribution of stress intensity $\bar{\sigma}_{11}$ of square laminated plates with $\theta = 30$ and 60 deg, respectively, and having a centrally located circular cutout of size $d/b = 0.2$. The plates are subjected to uniaxial compressive loading and are supported with the SSSS boundary condition. Again, only two values of θ are chosen, to economize space. It is observed that

1) The stress distribution for 30-deg laminates is almost uniform throughout the plate, except near the hole, for which a high stress concentration exists.

2) For 60-deg ply orientation, plate boundaries become active, which causes a reduction in the intensity of stress toward the center of the plate. As a result, stress near the load-carrying boundaries becomes significant. Also, stress concentration near the hole is not as pronounced as for 30-deg plates.

Prebuckling stiffness can be higher for SSSS plates with $\theta = 45$, 60, or 75 deg than for plates with other ply orientations (figure not shown). Plates with the SCSC boundary condition generally show

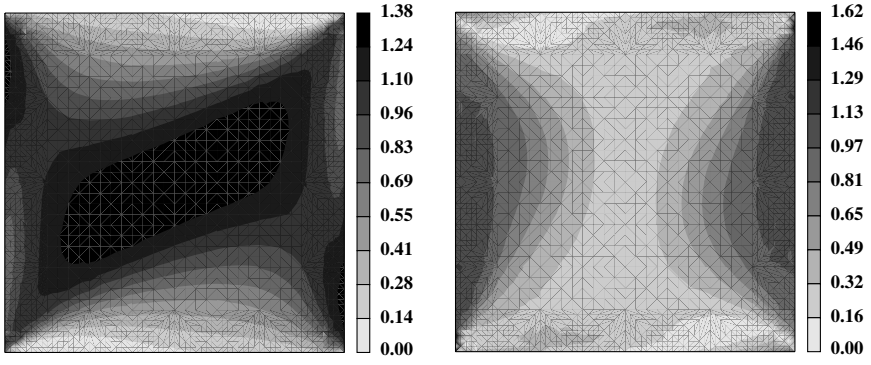

Fig. 3 Distribution of the intensity of stress $\bar{\sigma}_{11}$ for $-\theta/\theta$ square plates under uniaxial compression with the SSSS boundary condition and having different ply orientations: a) 30 deg and b) 60 deg.

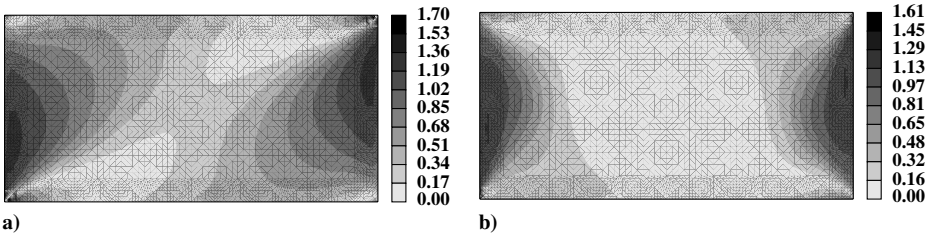

Fig. 4 Distribution of the intensity of stress $\bar{\sigma}_{11}$ for $-\theta/\theta$ rectangular plates ($a/b = 2$) under uniaxial compression with the SSSS boundary condition and having different ply orientations: a) 30 deg and b) 60 deg.

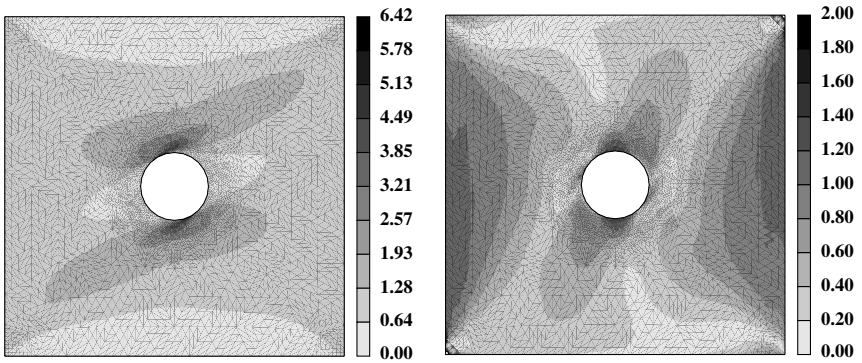

Fig. 5 Distribution of the intensity of stress $\bar{\sigma}_{11}$ for $-\theta/\theta$ square perforated plates under uniaxial compression with the SSSS boundary condition and having different ply orientations: a) 30 deg and b) 60 deg.

more significant effect on prebuckled stress than that of the SSSS case (figure not shown). However, plates with SFSF boundary constraints do not play any role in increasing the prebuckling stiffness of the plates compared with SSSS and SCSC plates. In this case, prebuckling stiffness is higher for 0-deg laminates and it decreases monotonically as ply orientation goes from 0 to 90 deg. The effect of the prebuckling stiffness on the mean buckling strength is discussed in the next section.

Comparison of the Mean Buckling Load

The mean buckling load for plates without cutouts, based on the layerwise plate model, using prebuckled stresses is compared with the Reddy and Khedir [4] analytical results based on the uniform-stress assumption. Table 2 shows the normalized mean buckling load of two-layered antisymmetric cross-ply square laminates with $b/h = 10$ and having different boundary conditions. The material properties used here are $E_{ll} = 40E_{tt}$, $G_{lt} = 0.6E_{tt}$, $G_{tt} = 0.5E_{tt}$, $\nu_{lt} = \nu_{tt} = 0.25$, and $E_{tt} = 10$ GPa. The buckling load obtained using the equivalent-layer model and based on the uniform prebuckled stress assumptions is also presented in the table. It is observed that

1) The mean buckling load obtained using the uniform-stress assumption and the equivalent-single-layer model lies between the values obtained using FSDT and HSDT [4]. CPT grossly overpredicts the buckling load.

2) The conventional 2-D plate models overpredict buckling loads compared with those obtained with the layerwise plate model.

3) The differences in the buckling loads obtained from the present layerwise model (with actual prebuckled stress) and conventional HSDT plate model [4] are found to be more significant (around 13%) for the SCSC boundary condition than for SSSS (around 5%) and SFSF (around 6%) boundary conditions. This is due to the increased effect of the boundary constraint in the case of the SCSC boundary condition compared with the other two boundary conditions.

The difference between the present and the conventional plate solutions is significant because the uniform-stress assumption neglects all other in-plane and out-of-plane stresses, which are significant for thick plates.

Validation for Statistics of the Buckling Load

To validate the SFEM implementation, the statistics of the buckling load obtained using the layerwise plate model is validated with the analytical solutions [35]. Table 3 shows the effect of variation in the material properties by adopting a coefficient of variation (COV), as defined in [35], on the buckling load for a thin single-layered orthotropic plate with $b/h = 100$ and having the

Table 2 Comparison of the nondimensioned mean buckling load for 0/90-deg square laminates having different support conditions and $b/h = 10$.

Various boundary conditions	Normalized mean buckling load $\bar{N} = \lambda_0^{cr} b^2/(E_{tt}h^3)$		
	Present result		Reddy and Khedir [4] result (various 2-D plate models)
	Using prebuckled stress (layer by layer)	Using uniform stress (equivalent layer)	
SSSS	11.070	11.525	11.562 (HSDT) 11.353 (FSDT) 12.957 (CPT)
SCSC	18.746	20.825	21.464 (HSDT) 20.067 (FSDT) 31.280 (CPT)
SFSF	4.625	4.931	4.940 (HSDT) 4.851 (FSDT) 5.425 (CPT)

Table 3 Influence of dispersion in material property on the SD of the buckling load for simply supported specially orthotropic plates with different aspect ratios and $b/h = 100$

Aspect ratio a/b	SD of the buckling load, MPa		
	Layerwise plate model		Analytical result [35] (with uniform stress)
	Using prebuckled stress	Using uniform stress	
1.0	0.917	0.915	0.916
2.0	0.656	0.523	0.524
3.0	0.608	0.507	0.508

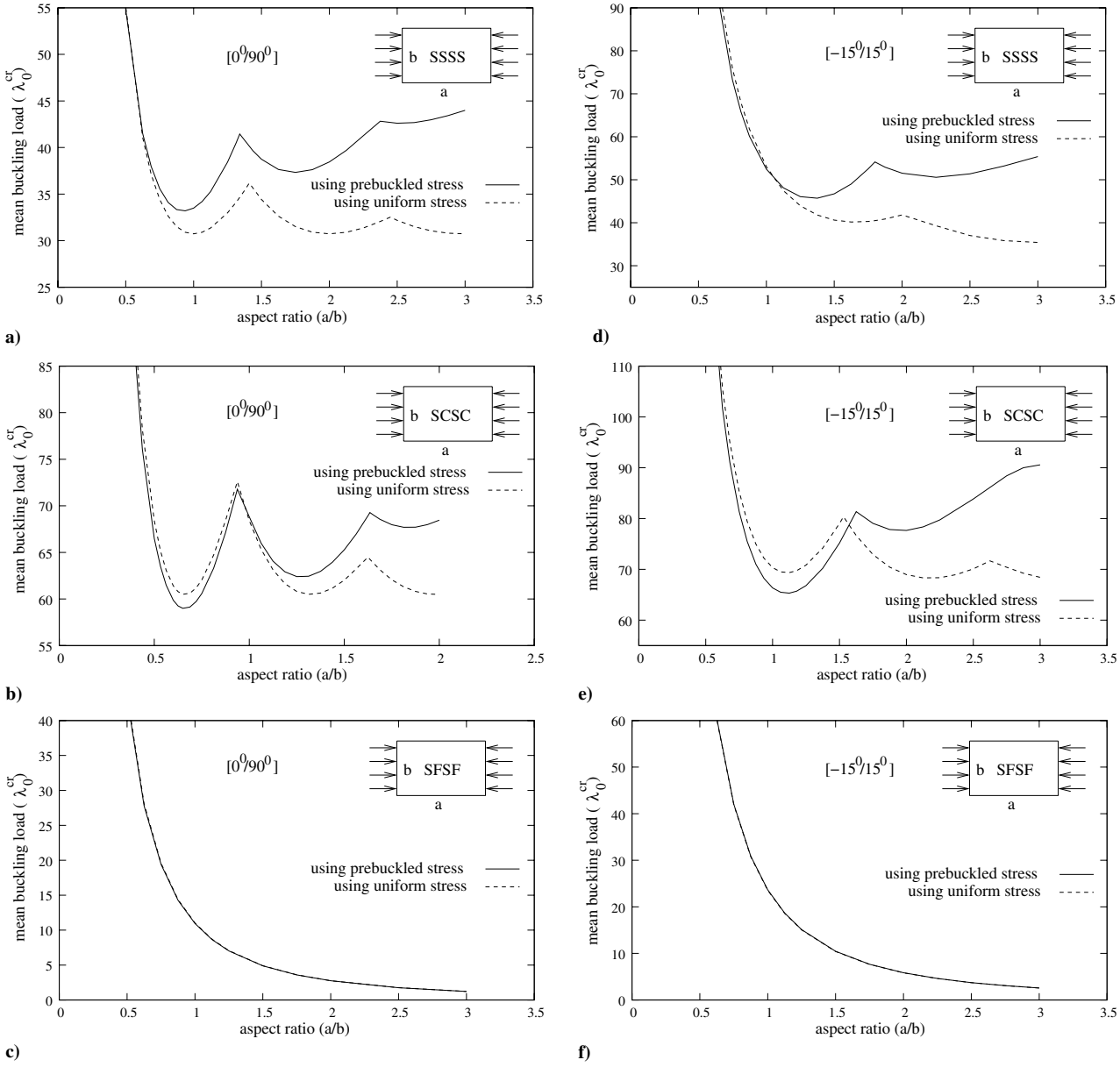

Fig. 6 Influence of aspect ratio on mean critical buckling load for 0/90-deg laminates with a) SSSS, b) SCSC, c) SFSF, and for −15/15-deg laminates with d) SSSS, e) SCSC, and f) SFSF boundary constraints.

SSSS boundary condition. The effect of both prebuckled-stress and uniform-stress assumptions on the statistics of the buckling-load parameter is shown. From the table it is observed that

1) The SD of the buckling load obtained using the layerwise model by assuming uniform state of stress is very close to the analytical results.

2) Stochastic analysis based on the uniform-stress assumption predicts lower SD of the buckling load than that based on prebuckled-stress analysis.

3) The difference between the SD of the buckling load using both assumptions becomes more significant as the aspect ratio of the plate increases.

The layerwise plate model, using the uniform-stress assumption, gives slightly lower SD of the buckling load than the closed-form value, because this model is less stiff than the Kirchhoff–Love model. This validates the SFEM implementation of the present study.

Mean Buckling Load

In this section, results for the mean buckling load of two-layered antisymmetric plates under uniaxial compressive and shear loading and various boundary conditions are presented. First, the mean buckling behavior of unperforated laminated plates is studied and then the effect of the presence of both circular and elliptical cutouts on the mean buckling behavior of plates is presented.

Plates Without Cutouts

Here, we first discuss the effect of the prebuckled-stress as opposed to the uniform-stress assumption on the mean buckling behavior of 0/90- and −15/15-deg unperforated plates under uniaxial compressive loading. Subsequently, the effect of ply orientation θ on the mean buckling load of $-\theta/\theta$ plates under shear and compression using prebuckled stress is presented.

Figures 6a–6f show the effect of plate aspect ratios on the mean critical buckling load of 0/90- and −15/15-deg laminated plates under the SSSS, SCSC, and SFSF boundary conditions. The effects of both the prebuckled-state-of-stress and uniform-stress assumptions on the mean buckling behavior are presented. From the figures, it is observed that

1) In the case of SSSS plates, the uniform-stress assumption always predicts a lower buckling load than the actual prebuckled-

stress-based buckling load for all aspect ratios. For example, the difference in the buckling load using prebuckled analysis and uniform-stress assumption is about 30% for 0/90-deg plates and 36% for −15/15- deg plates at $a/b = 3$.

2) The mean buckling behavior of SCSC plates is slightly different from SSSS plates.

3) The mean buckling loads are progressively higher at higher plate aspect ratios with the prebuckled-stress analysis than those with the uniform-stress assumption for both SSSS and SCSC plates. This is due to the presence of diffusion in the intensity of stress inside the plate, which becomes more significant at higher plate aspect ratios (see Figs. 3 and 4).

4) SFSF plates give similar buckling behavior with both prebuckled- and uniform-stress assumptions. This is because the actual prebuckled stress is essentially uniform normal stress throughout the plate. The buckling load also decreases monotonically with an increase in the aspect ratio of the plates.

The reason for getting completely different buckling behavior for SSSS and SCSC plates using both uniform- and prebuckled-stress assumptions is that the prebuckled-stress solution has all six components, whereas in the uniform-stress assumption, $\bar{\sigma}_{11} = 1$ is taken as the only nonzero stress in the prebuckled state. Moreover, the distribution of intensity $\bar{\sigma}_{11}$ shows diffusion or reduction in stress from the loaded edge toward the middle of the plate, which becomes more significant at higher plate aspect ratios. As a result, the maximum stress at the center of the plate is reduced and stresses near the edges are increased. Because the edges are constrained, this stress increase near the edges may cause the plate to sustain higher buckling loads. That is why the buckling loads are progressively higher at higher plate aspect ratios. However, in the case of SFSF plates, the effect of constraints due to the boundary is much less than that with SSSS and SCSC plates, which allows the plate to have a uniform state of stress everywhere. This example shows how the uniform-stress assumption can wrongly predict the mean buckling behavior of plates under uniaxial compressive loading. The rest of the numerical examples presented in this paper will be only based on the actual prebuckled state of stress.

Now we discuss the effect of ply orientation θ on the mean buckling load for $-\theta/\theta$ laminated plates under uniaxial compressive loading. Figure 7 shows the effect of θ for square plates with SSSS, SCSC, and SFSF boundary conditions. It is observed that

1) The variation in the mean buckling load due to variation in θ is significant and is about 42% for plates with the SSSS boundary condition. Plates with $\theta \approx 30$ deg have the minimum and plates with $\theta \approx 55$ deg have the maximum buckling loads.

2) The variation in the mean buckling load for SCSC plates due to variation in θ is around 30%, with the minimum at $\theta \approx 25$ deg and the maximum at $\theta \approx 60$ deg.

3) The mean buckling load of SCSC plates is always higher for any ply orientation than that of SSSS plates.

4) The mean buckling load of SFSF plates decreases monotonically as θ increases from 0 to 90 deg. The variation in the buckling load is about 90%, with the minimum at 90-deg plates and the maximum at 0-deg plates. These plates always exhibit a lower buckling load than that with SSSS and SCSC plates.

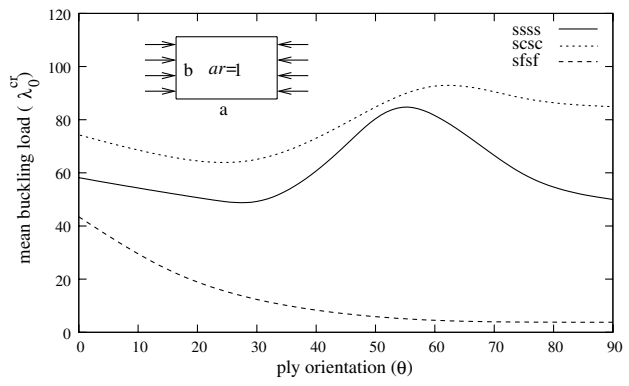

Fig. 7 The effect of ply orientation on the mean critical buckling load for $-\theta/\theta$ square plates with different boundary conditions.

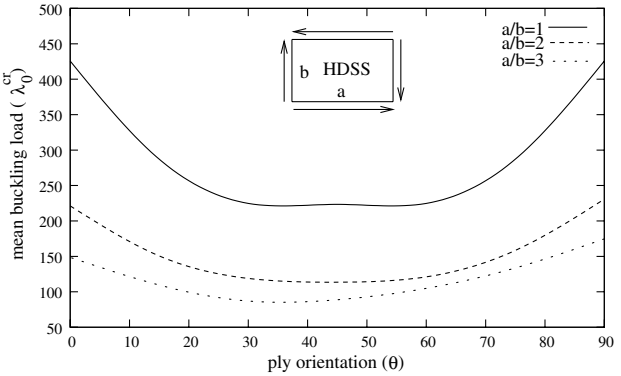

Fig. 8 The effect of ply orientation on the mean critical buckling load for $-\theta/\theta$ square plates under shear loading with different aspect ratios.

Both SSSS and SCSC boundary conditions increase the prebuckling stiffness of plates for $\theta > 30$ deg. It is also seen that the prebuckling stiffness is always higher for plates with the SCSC boundary condition than for SSSS plates. That is why SCSC plates always show a higher mean buckling load than that with SSSS plates. Because the effect of constraint on prebuckling stiffness is less for SFSF plates, these plates show a lower buckling load than that with other plates. It may be noted that SFSF plates show the maximum variation in the buckling load due to a change in θ compared with plates with SSSS and SCSC boundary conditions.

In the preceding study, we discussed the mean buckling behavior of unperforated plates under uniaxial compression. Figure 8 shows the effect of θ on the buckling behavior of a shear-loaded plate with different aspect ratio. It is observed that

1) Plates under shear loading have a higher mean buckling load than plates under axial compressive loading for all aspect ratios. For example, plates with $\theta = 0$ deg have about a seven-times-higher buckling load than that of axially loaded plates with the SSSS boundary condition. This is because for shear-loaded plates, most of the stress is found near the corner of the boundaries. Because the corners are restrained, these plates can take more loads than can plates under compressive loading.

2) A symmetry in the mean buckling behavior exists for plates with $a/b = 1$ and it is minimum at $\theta = 45$ deg and maximum for 0- and 90-deg plates. However, this symmetry in buckling behavior is distorted as the aspect ratio increases.

3) There is a monotonic reduction in the buckling load with increasing aspect ratio for each laminate type; reductions of approximately 50% in the buckling load are found as the aspect ratio of the plate increases from $a/b = 1$ to 2. This may be due to an increase in the area of the loaded edge.

The basic behavior of shear-loaded plates is different from the behavior of compression-loaded plates. This difference is more readily understood by replacing the shear load acting on a plate with the equivalent pairs of diagonal tension and compression forces. By using this, it is seen that a substantial portion of the destabilizing compressive force acting in a shear-loaded plate is centrally located. The shear buckling loads are found lower for laminates with $\theta = 30$, 45, and 60 deg. For these laminates, the fibers in the bottom ply are closely aligned with the compression diagonal of the plate. The lowest buckling load is predicted for the laminate with $\theta = 45$ deg. In this case, the fibers in the bottom ply are exactly aligned with the compression diagonal of the plate.

Plates with Cutouts

In this section, we first study the mean buckling behavior of $-\theta/\theta$ square plates in the presence of a centrally located circular cutout under uniaxial compression. Figure 9 shows the effect of ply orientation on the mean buckling load of plates with a cutout size $d/b = 0.2$ having SSSS, SCSC, and SFSF boundary conditions. It is observed that

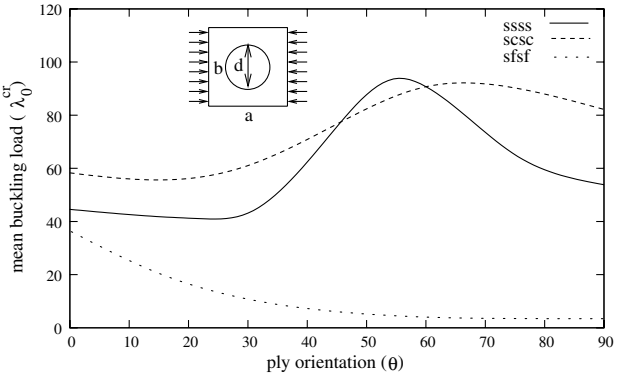

Fig. 9 The effect of ply orientation on the mean critical buckling load for $-\theta/\theta$ square plates with a cutout having different boundary conditions.

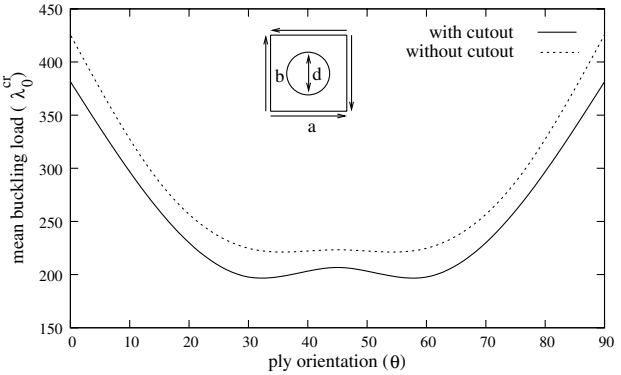

Fig. 10 The effect of ply orientation on the mean critical buckling load for $-\theta/\theta$ square plates with and without cutouts under shear loading.

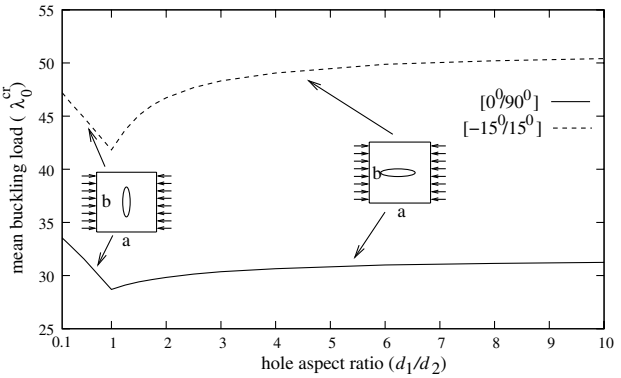

Fig. 11 The effect of the hole aspect ratio d_1/d_2 on the mean critical buckling load for 0/90- and $-15/15$-deg square plates under the SSS boundary condition.

1) The mean buckling load of plates generally decreases in the presence of a cutout compared with unperforated plates. However, the mean buckling load of perforated plates with θ lying between 45–90 deg is found to be higher than that of unperforated plates having the SSSS boundary condition.

2) The SCSC boundary condition does not play any significant role in increasing the prebuckling stiffness of plates in the presence of a cutout, as opposed to plates with SSSS plates with some particular ply orientation.

3) The mean buckling load of plates with a cutout under both SSSS and SCSC boundary conditions decreases slightly, up to $\theta \approx 25$ deg. This is because the stress concentration near the hole increases with an increase in θ, which results in a monotonic reduction in the prebuckling stiffness of the plates.

4) The mean buckling load of plates with 45-, 60-, 75-, and 90-deg ply orientation under both SSSS and SCSC boundary conditions is higher than that of 0-, 15- and 30-deg plates. This is because the effect of boundary constraints is found to be significant in these cases.

5) The buckling load is maximum for plates with $\theta \approx 55$ deg under the SSSS and $\approx$65 deg under the SCSC boundary condition.

6) The buckling load of SCSC plates with a cutout is generally higher than that of plates with the SSSS boundary condition, except for θ, which lies between 45–60 deg. The prebuckling stiffness is generally higher for SCSC plates than for plates with the SSSS boundary condition. But for θ lying between 45–60 deg, the presence of a cutout develops a tensile zone near it, which increases the prebuckling stiffness of the plates.

7) For plates with the SFSF boundary condition, the mean buckling load decreases monotonically with an increase in ply orientation. This is because the stress concentration near the hole increases with an increase in θ, which results in a monotonic reduction in prebuckling stiffness with an increase in θ.

The presence of a centrally located cutout in plates results in a loss of bending stiffness in the central region. When such a plate is loaded axially, the bending stiffness in the central part of the plate is of great importance. As discussed earlier, boundary constraints play a very significant role that significantly changes the prebuckling stiffness and thus the buckling resistance of the plates. When a cutout is present, the bending stiffness in the central region of the plate reduces under all three types of boundary constraints. However, in the case of SSSS boundary constraints, the effect of the loss of central bending stiffness can be reduced by a proper choice of ply orientation, which increases the buckling resistance of the plate.

The buckling behavior of shear-loaded square laminated plates $-\theta/\theta$ in the presence of a centrally located circular cutout of size $d/b = 0.2$ is also studied and shown in Fig. 10. It is observed that

1) The mean buckling behavior has almost the same pattern as that observed for plates without cutouts. Here, the mean buckling load of 45-deg plates is slightly higher than that of 30- and 60-deg plates.

2) The mean buckling load of plates decreases in the presence of a cutout for all ply orientations compared with unperforated plates.

It is already seen that a substantial portion of the destabilizing compressive force acting in a shear-loaded plate is centrally located. In this situation, the buckling behavior is strongly dependent on the loss of bending stiffness in the central portion of a plate because of the presence of a cutout. Hence, the shear buckling load is dominated by the loss in bending stiffness (i.e., the shear buckling load decreases in the presence of a cutout).

Consider that the size of a cutout is reduced by reducing the vertical diameter d_2 of the hole and keeping the horizontal diameter d_1 fixed. This reduction in hole size basically leads to an elliptical cutout, which on further reductions, ultimately leads to a horizontal crack through the thickness in the plate. Similarly, we can also have a vertical through-the-thickness crack in the plate by reducing the horizontal diameter of the hole while keeping the vertical diameter fixed. Figure 11 shows the effect of the aspect ratio d_1/d_2 of such a hole on the mean buckling strength of 0/90- and $-15/15$-deg square plates with the SSSS boundary condition under uniaxial compressive loading. Plates with such elliptical cutouts generally show an increase in critical buckling load for any d_1/d_2 ratio (i.e., both horizontally or vertically orientated elliptical cutouts) compared with a circular cutout with $d_1/d_2 = 1$. Hence, the buckling capacity of the plate can be substantially enhanced by increasing or decreasing the aspect ratio of the hole.

Variance of the Buckling Load

In this section, the effect of variation in the effective material properties is presented, obtained from the micromechanics-based approach [36] on the second-order statistics of the buckling load for plates with and without cutouts. The COV obtained from micromechanics approach for E_{ll}, E_{tt}, ν_{lt}, ν_{tt}, G_{lt}, and G_{tt} are 7, 4, 4, 4, 12, and 3%, respectively. Using these statistics, the influence of all BRVs changing simultaneously on the COV of the buckling load for $-\theta/\theta$ square plates without cutouts under uniaxial compression is calculated and depicted in Fig. 12. Three different boundary conditions (SSSS, SCSC, and SFSF) are taken. It is observed that

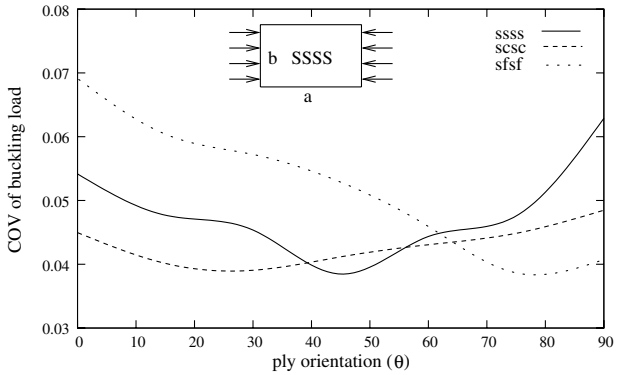

Fig. 12 Influence of dispersion in all material properties changing simultaneously on the COV of the critical buckling load for $-\theta/\theta$ square laminates with different ply orientations and boundary conditions.

1) In the case of the SSSS boundary condition, the COV of the buckling load is minimum at $\theta = 45$ deg and maximum at 90-deg laminates. For this plate, the COV of the buckling load is almost symmetrical (about $\theta = 45$ deg) and lies between 4–7%.

2) The COV of the buckling load for plates with the SCSC boundary condition is found between 4–5% for all cases studied. For this case, the change in ply orientation has less effect on the COV of the buckling load than that with other boundary conditions.

3) For SFSF plates, the COV of the buckling load is maximum for 0-deg ply orientation and it decreases as θ changes from 0 to 90 deg. For this case, the COV of the buckling load lies between 4–7%.

The influence of BRVs, all with the same statistics as defined earlier, on the COV of the buckling load for $-\theta/\theta$ square plates in the presence of a cutout under uniaxial compression is presented in Fig. 13. All three boundary conditions (SSSS, SCSC, and SFSF) are taken. It is observed that

1) The COV of the buckling load is generally higher for plates with a cutout than that for unperforated plates.

2) The COV of the buckling load for both SSSS and SFSF plates lies between 2–12%.

3) The behavior pattern of the COV of the buckling load for all three cases is completely different from the unperforated plates.

4) Changes in the ply orientation for plates with SCSC boundary constraints have less effect on the COV of the buckling load, which lies between 6–10%.

The influence of simultaneous change in all BRVs on the critical buckling load is also studied for shear-loaded plates with and without cutouts and shown in Fig. 14. In this case, the HDSS boundary condition is taken. It is observed that

1) Plates with a cutout show a higher COV of the buckling load than that for plates without cutouts. However, the behavior pattern of the COV of the buckling load is similar for both cases. The COV of the buckling load for plates with a cutout is less sensitive to change in the ply angle.

2) The COV of the buckling load is between 3–6.5% for plates with a cutout, whereas for unperforated plates it lies between 3–4%.

3) The COV of the buckling load is minimum at $\theta = 0$ and 90 deg and maximum at $\theta \approx 30$ and 60 deg.

In the previous case, we studied the effect of the size of a cutout by reducing the vertical diameter d_2 of the hole and keeping the horizontal diameter d_1 of the hole fixed and vice versa on the mean buckling load of the two-layered laminate system. Now the effect of the elliptical cutout aspect ratio on the COV of the buckling load is examined for the same laminate system (i.e., 0/90 deg and $-15/15$-deg under uniaxial compressive loading). The SSSS boundary condition is taken. From Fig. 15, it can be observed that for changes in d_1/d_2 from 0.1 to 10,

1) The COV of the buckling load for 0/90-deg laminates lies between 8–11%, whereas for $-15/15$-deg laminates it lies between 6–8%.

2) Plates with a circular cutout ($d_1/d_2 = 1$) have the maximum COV in the buckling load compared with plates with elliptical cutouts (both horizontal and vertical).

3) Plates with a horizontal crack ($d_1/d_2 = 10$) have a smaller COV of the buckling load than that of vertically cracked ($d_1/d_2 = 0.1$) plates for both of the cases studied.

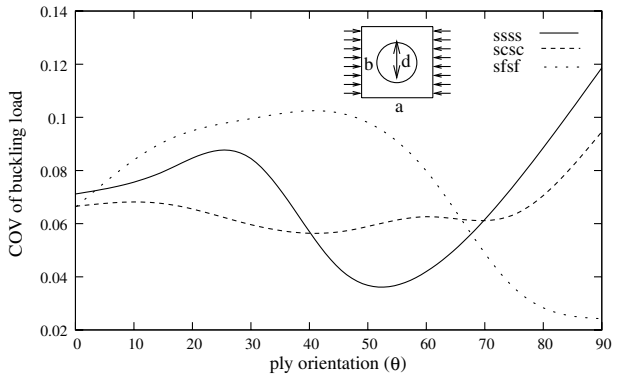

Fig. 13 Influence of dispersion in all material properties changing simultaneously on the COV of the critical buckling load for $-\theta/\theta$ square laminates with a cutout having different ply orientations and boundary conditions.

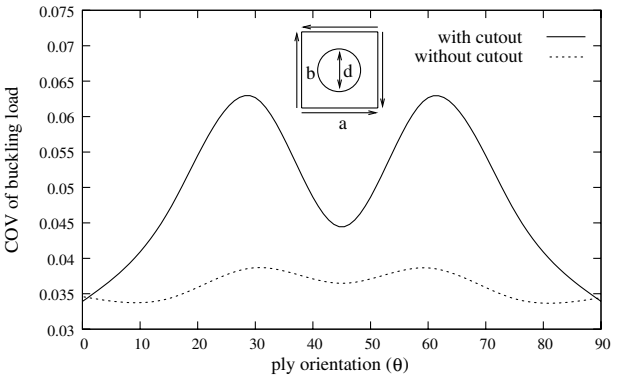

Fig. 14 Influence of dispersion in all material properties changing simultaneously on the COV of the critical buckling load for $-\theta/\theta$ square laminates with different ply orientations under shear loading.

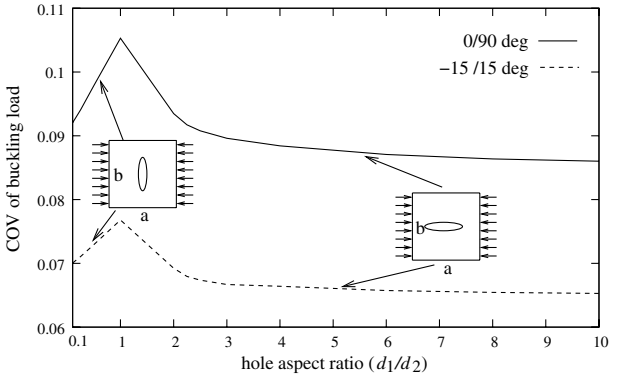

Fig. 15 Influence of dispersion in all material properties changing simultaneously on the COV of the critical buckling load for 0/90- and $-15/15$-deg square laminates with different hole aspect ratio d_1/d_2 and SSSS boundary condition.

Conclusions

In this work, an attempt was made to study the statistics of the critical buckling-load parameters of composite plates with and without cutouts. From the numerical results, the following conclusions can be drawn:

1) The prebuckled state of stress is strongly influenced by the applied boundary conditions, plate aspect ratio, and ply orientation. Hence, the mean buckling load attained by the current analysis using prebuckled stress can be completely different from that reported in the literature, assuming a uniform state of stress.

2) Plates under shear loading have a higher mean buckling load than that of plates under uniaxial compression.

3) The mean buckling load of plates generally decreases in the presence of a cutout compared with unperforated plates. However, perforated plates under uniaxial compression with some specific boundary condition and layup sequences show a higher buckling load than that of unperforated plates.

4) Plates with elliptical cutouts (both horizontal and vertical) generally show an increase in critical buckling load compared with plates with a circular cutout.

5) In most cases, the COV of the buckling load for the applied variation in material properties lies between 6–10%.

6) Plates with a cutout show a higher COV of the buckling load than that of plates without cutouts.

7) Plates with a circular cutout have the maximum COV in the buckling load compared with plates with elliptical cutouts (both horizontal and vertical).

8) In the design process, the effect of dispersion in the material parameters on the buckling load has to be accounted for. Because of material dispersion, the buckling load exhibits a scatter and buckling can happen at load levels that are significantly lower than those of the mean buckling load.

References

[1] Timoshenko, S. P., and Gere, J. M., "Theory of Elastic Stability," *Engineering Society Monographs*, McGraw–Hill, New York, 1961.

[2] Jones, R. M., "Mechanics of Composite Materials," Scripta, Washington, D.C., 1975.

[3] Reddy, J. N., and Phan, N. S., "Stability and Natural Vibration of Isotropic, Orthotropic and Laminated Plates According to a Higher Order Shear Deformable Theory," *Journal of Sound and Vibration*, Vol. 98, No. 2, 1985, pp. 157–170.

[4] Reddy, J. N., and Khedir, A. A., "Buckling and Vibration of Laminated Composite Plates Using Various Plate Theories," *AIAA Journal*, Vol. 27, No. 12, 1989, pp. 1808–1817.

[5] Gu, H., and Chattopadhyay, A., "Three-Dimensional Elasticity Solution for Buckling of Composite Laminates," *Composite Structures*, Vol. 50, No. 1, 2000, pp. 29–35.

[6] Leissa, A. W., and Kang, J., "Exact Solutions for Vibration and Buckling of an SS-C-SS-C Rectangular Plate Loaded by Linearly Varying In-Plane Stresses," *International Journal of Mechanical Sciences*, Vol. 44, No. 9, 2002, pp. 1925–1945.

[7] Hu, H., Badir, A., and Abatan, A., "Buckling Behavior of a Graphite/Epoxy Composite Plate Under Parabolic Variation of Axial Loads," *International Journal of Mechanical Sciences*, Vol. 45, No. 6, 2003, pp. 1135–1147.

[8] Zienkiewicz, O. C., *The Finite Element Method*, McGraw–Hill, London, 1977.

[9] Cook, R. D., *Concepts and Applications of Finite Element Analysis*, Wiley, New York, 1981.

[10] Nair, S., Singh, G., and Rao, G. V., "Stability of Laminated Composite Plates Subjected to Various Types of In-Plane Loading," *International Journal of Mechanical Sciences*, Vol. 38, No. 2, 1996, pp. 191–202.

[11] Sundaresan, P., Singh, G., and Rao, G. V., "Buckling of Moderately Thick Rectangular Composite Plates Subjected to Partial Edge Compression," *International Journal of Mechanical Sciences*, Vol. 40, No. 11, 1998, pp. 1105–1117.

[12] Matsunaga, H., "Vibration and Stability of Angle-Ply Laminated Composite Plates Subjected to In-Plane Stresses," *International Journal of Mechanical Sciences*, Vol. 43, No. 8, 2001, pp. 1925–1944.

[13] Gilat, R., Williams, T. O., and Aboudi, J., "Buckling of Composite Plates by Global-Local Plate Theory," *Composites, Part B*, Vol. 32, No. 3, 2001, pp. 229–236.

[14] Nemeth, M. P., "Buckling of Long Compression-Loaded Anisotropic Plates Restrained Against In-Plane Lateral and Shear Deformations," *Thin-Walled Structures*, Vol. 42, No. 5, 2004, pp. 639–685.

[15] Yettram, A. L., and Brown, C. J., "The Elastic Stability of Square Perforated Plates Under Biaxial Loadings," *Computers and Structures*, Vol. 22, No. 4, 1986, pp. 589–594.

[16] Nemeth, M. P., Stein, M., and Johnson, E. R., "An Approximate Buckling Analysis for Rectangular Orthotropic Plates with Centrally Located Cutouts," NASA, TP 2528, 1986.

[17] Nemeth, M. P., "Importance of Anisotropy on Buckling of Compression Loaded Symmetric Composite Plates," *AIAA Journal*, Vol. 24, No. 11, 1986, pp. 1831–1835.

[18] Larsson, P. L., "On Buckling of Orthotropic Compressed Plates with Circular Holes," *Composite Structures*, Vol. 7, No. 2, 1987, pp. 103–121.

[19] Lin, C. C., and Kuo, C. S., "Buckling of Laminated Plates with Holes," *Journal of Composite Materials*, Vol. 23, No. 6, 1989, pp. 536–553.

[20] Srivasta, K. S., and Krishnamurthy, A. V., "Stability of Laminated Composite Plates with Cut-Outs," *Computers and Structures*, Vol. 43, No. 2, 1992, pp. 273–279.

[21] Sabir, A. B., and Chow, F. Y., "Elastic Buckling of Plates Containing Eccentrically Located Circular Holes," *Thin-Walled Structures*, Vol. 4, No. 2, 1986, pp. 135–150.

[22] Shakerley, T. M., and Brown, C. J., "Elastic Buckling of Plates with Eccentrically Positioned Rectangular Perforations," *International Journal of Mechanical Sciences*, Vol. 38, Nos. 8–9, 1996, pp. 825–838.

[23] Noor, A. K., and Kim, Y. H., "Buckling and Postbuckling of Composite Panels with Cutouts Subjected to Combined Edge Shear and Temperature Change," *Computers and Structures*, Vol. 60, No. 2, 1996, pp. 203–222.

[24] Bailey, R., and Wood, J., "Postbuckling Behavior of Square Compression Loaded Graphite Epoxy Panels with Square and Elliptical Cutouts," *Thin-Walled Structures*, Vol. 28, Nos. 3–4, 1997, pp. 373–397.

[25] Nemeth, M. P., "Buckling Behavior of Compression Loaded Symmetrically Laminated Angle-Ply Plates with Holes," *AIAA Journal*, Vol. 26, No. 3, 1988, pp. 330–336.

[26] Zhang, J., and Ellingwood, B., "Effects of Uncertain Material Properties on Structural Stability," *Journal of Structural Engineering*, Vol. 121, No. 4, 1995, pp. 705–716.

[27] Lin, S. C., "Buckling Failure Analysis of Random Composite Laminates Subjected to Random Loads," *International Journal of Solids and Structures*, Vol. 37, No. 51, 2000, pp. 7563–7576.

[28] Kleiber, M., and Hien, T. D., *The Stochastic Finite Element Method*, Wiley, New York, 1992.

[29] Elishakoff, I., "Uncertain Buckling: Its Past, Present and Future," *International Journal of Solids and Structures*, Vol. 37, No. 46, 2000, pp. 6869–6889.

[30] Grigoriu, M., "Stochastic Mechanics," *International Journal of Solids and Structures*, Vol. 37, Nos. 1–2, 2000, pp. 197–214.

[31] Argyris, J., Papadrakakis, M., and Stefanou, G., "Stochastic Finite Element Analysis of Shells," *Computer Methods in Applied Mechanics and Engineering*, Vol. 191, No. 41, 2002, pp. 4781–4804.

[32] Stefanou, G., and Papadrakakis, M., "Stochastic Finite Element Analysis of Shells with Combined Random Material and Geometric Properties," *Computer Methods in Applied Mechanics and Engineering*, Vol. 193, Nos. 1–2, 2004, pp. 139–160.

[33] Ahmad, N. U., and Basu, P. K., "Higher-Order Finite Element Modeling of Laminated Composite Plates," *International Journal for Numerical Methods in Engineering*, Vol. 37, No. 1, 1994, pp. 123–139.

[34] Actis, R. L., Szabo, B. A., and Schwab, C., "Hierarchic Models for Laminated Plates and Shells," *Computer Methods in Applied Mechanics and Engineering*, Vol. 172, No. 1, 1999, 79–107.

[35] Onkar, A. K., Upadhyay, C. S., and Yadav, D., "Generalized Buckling Analysis of Laminated Plates with Random Material Properties Using Stochastic Finite Elements," *International Journal of Mechanical Sciences*, Vol. 48, No. 7, 2006, pp. 780–798.

[36] Onkar, A. K., Upadhyay, C. S., and Yadav, D., "Stochastic Finite Element Buckling Analysis of Laminated Composite Plates with Circular Cutout Under Uniaxial Compression," *Journal of Applied Mechanics* (to be published).

A. Roy
Associate Editor